JOC Article

Experimental and Computational Studies of the Recognition of Amino Acids by Galactosyl-imine and -amine Derivatives: An Attempt to Understand the Lectin−Carbohydrate Interactions

Rohit Ahuja,[†] Nitin K. Singhal,[†] Balaji Ramanujam,[†] Maddula Ravikumar,[‡] and Chebrolu P. Rao*,[†]

Bioinorganic Laboratory, Department of Chemistry, Indian Institute of Technology Bombay, Mumbai 400 076, India, and Analytical Chemistry Division, Indian Institute of Chemical Technology, Hyderabad 500 007, India

cprao@iitb.ac.in

Received January 17, 2007

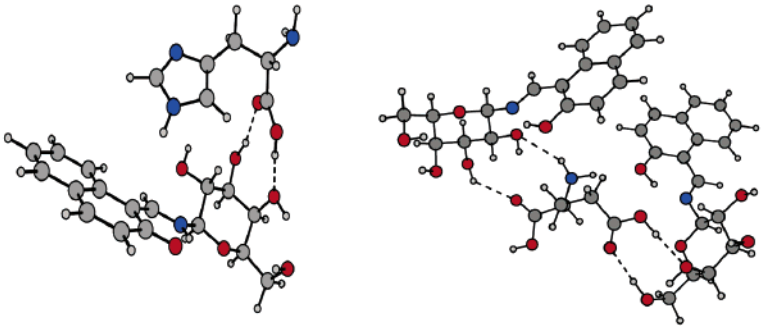

GNI...His **GNI...Glu...GNI**

A galactosyl-naphthyl-imine-based derivative, 1-(β-D-galactopyranosyl-1′-deoxy-1′-iminomethyl)-2-hydroxynaphthalene (**GNI**), and a galactosyl-naphthyl-amine-based derivative, 1-(galactopyranosyl-1′-deoxy-1′-aminomethyl)-2-hydroxynaphthalene (**GNA**), possessing an ONO binding core were studied for their recognition of naturally occurring amino acids using fluorescence and absorption spectroscopy, and the corresponding association constants were derived for the complexes formed. The complexes formed between **GNI**/**GNA** and amino acids were supported by electrospray ionization mass spectrometry (ESI/MS). The structures of the complexes were optimized by computational studies using density functional theory, and stabilization energies were computed for the complexes to substantiate the interactions present between **GNI**/**GNA** and amino acid. The interactions were found to be primarily hydrogen bonding in nature. These interactions are reminiscent of those present in the lectin-carbohydrate and glycosidase substrate. Thus, the carbohydrate moiety present in **GNI** shows high specificity toward the −COOH group of the amino acid, which may be relevant to such interactions present between the carbohydrates and the polypeptides.

Introduction

Lectins are carbohydrate-binding proteins of nonimmune origin that agglutinate cells and/or precipitate glycoconjugates and are isolated mainly from plant and animal sources.[1] These serve many different biological functions and are known to play important roles in the immune system found exclusively on pathogens/cell surfaces.[2] As a result of this, lectins are potentially involved in a wide range of applications in the fields of pharmacology, immunology, and cancer therapy.[3] In all these, the main property of the lectin is to recognize carbohydrates

* To whom correspondence should be addressed. Phone: 91 22 2576 7162. Fax: 91 22 2572 3480.
[†] Department of Chemistry, Indian Institute of Technology Bombay.
[‡] Analytical Chemistry Division, Indian Institute of Chemical Technology.

(1) (a) Ahuja, R.; Singhal, N. K.; Rao, C. P. *Khim./Chem.: Bulgarian J. Chem. Educ.* **2006**, *15*, 275 and references cited therein. (b) Sharon, N. *Trends Biochem. Sci.* **1993**, *18*, 221. (c) Rini, J. M. *Annu. Rev. Biophys. Biomol. Struct.* **1995**, *24*, 551. (d) Audette, G. F.; Olson, D. J. H.; Ross, A. R. S.; Quail, J. W.; Delbaere, L. T. J. *Can. J. Chem.* **2002**, *80*, 1010.

10.1021/jo0700979 CCC: $37.00 © 2007 American Chemical Society
Published on Web 03/30/2007

SCHEME 1 [a]

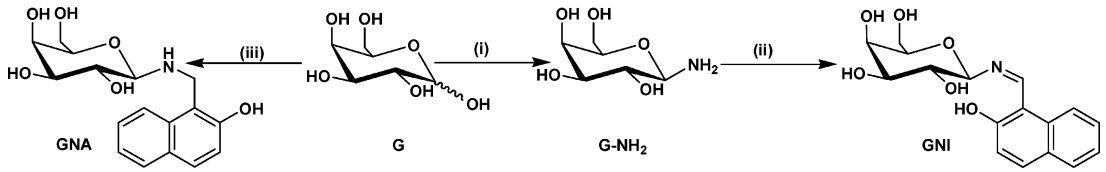

[a] Schematic representation of the synthesis of **G-NH2**, **GNI**, and **GNA** from **G** (i.e., galactose): (i) MeOH, NH_3 for 10 h at rt, store at +4 °C for 3 days; (ii) galactosyl-C1-deoxy-C1-amine (**G-NH$_2$**, 3.584 g, 20.02 mmol), 2-hydroxy-1-napthaldehyde (3.612 g, 20.88 mmol), EtOH, reflux, 8 h, yield of 4.91 g, 74%; (iii) galactose (1.80 g, 10 mmol), 1-aminomethyl-2-naphthol (1.78 g, 10.3 mmol), EtOH, reflux, 8 h, yield of 2.2 g, 66%.

selectively.[4] Recent literature witnessed reports on purification and characterization of a number of lectins isolated from different sources and comprising varying carbohydrate specificities.[5] Of these, several are galactose-based ones. On the basis of few crystal structures reported in the literature, it is reasonable to conclude that the recognition of carbohydrates by lectins is primarily through hydrogen bonding, though such interactions were yet to be proven in a large number of lectins.[6] On the other hand, glycosidases selectively hydrolyze glycosidic bonds where the substrate glycoside is expected to interact with the polypeptide in the active site. To model the interactions displayed by lectins and glycosidases toward carbohydrates, it would become critical to study the interactions present between carbohydrates and amino acids using both experimental and computational methods.

In our journey to understand the basis of the interactions of carbohydrates with lectins and glycosidases, we have taken up a model study involving the galactosyl-naphthyl-imine-based derivative, viz., 1-(β-D-galactopyranosyl-1′-deoxy-1′-iminomethyl)-2-hydroxynaphthalene (**GNI**), and the galactosyl-naphthyl-amine-based derivative, viz., 1-(galactopyranosyl-1′-deoxy-1′-aminomethyl)-2-hydroxynaphthalene (**GNA**), and naturally occurring amino acids using absorption and fluorescence spectroscopy, where the naphthyl moiety acts as an intrinsic chromophore as well as a fluorophore. The species formed between these derivatives and the amino acids were confirmed on the basis of electrospray ionization mass spectrometry (ESI/MS). The complexes formed were further studied by computational methods using Gaussian 98 and/or Gaussian 03 at varying levels of calculations, such as semiempirical (PM3), ab initio (HF), and density functional theory (B3LYP).

Results and Discussion

The galactosyl derivatives, viz., **GNI** and **GNA**, were synthesized as per that shown in Scheme 1. The details of the synthesis and the characterization data are presented in the Experimental Section.

A. Fluorescence Spectral Studies. Although free **GNA** exhibits one intense fluorescence emission peak centered at 355 nm, free **GNI** exhibits two weak emissions centered at 355 and 445 nm. Comparison of the fluorescence emission spectra of naphthalene, β-naphthol, 2-hydroxy-1-napthaldehyde, and **GNA** with that of **GNI** leads to the assignment of the 355 nm band to that arising from naphthalene and of the 445 nm band to that arising from a naphthalene in conjugation with an imine moiety (Supporting Information, S1). The presence of a lone pair on the nitrogen of −C═N− in **GNI** results in photoinduced electron transfer (PET) that quenches the fluorescence in **GNI** as compared to that in **GNA**. Both **GNI** and **GNA** were titrated against all 20 naturally occurring L-amino acids by fluorescence spectroscopy according to the titration details given in the Experimental Section.

Fluorescence Titration of GNI with Amino Acids. Fluorescence spectra obtained during the titration of **GNI** with Glu are shown in Figure 1a. The titration results in quenching the fluorescence of the 355 nm band as the ratio of the added Glu increases, however, show no significant change in the fluorescence of the 445 nm band, as can be noticed from the relative fluorescence ratio (I/I_0) plot given in Figure 1b. The results are clearly suggestive of the interaction of Glu with **GNI**. On the other hand, the titration of **GNI** with His, Leu, and Pro resulted in an increase of fluorescence intensity of both bands to varying extents (Supporting Information, S2), indicating that the interacting strengths with **GNI** vary among these amino acids. The I/I_0 plots for these titrations are shown in Figure 2. Thus, the fluorescence intensity was either enhanced or quenched depending upon the amino acid used in the titration of **GNI**.

All the remaining 16 amino acids showed no appreciable change in the fluorescence intensity of either band of **GNI** (Figure 3). The results thus clearly indicate selective association between **GNI** and the four amino acids, viz., Glu, His, Leu, and Pro, whereas the nature of the interaction seems to be

(2) (a) Lis, H.; Sharon, N. *Chem. Rev.* **1998**, *98*, 637. (b) Zhu-Salzman, K.; Hammen, P. K.; Salzman, R. A.; Koiwa, H.; Bressan, R. A.; Murdock, L. L.; Hasegawa, P. M. *Comp. Biochem. Physiol., B* **2002**, *132*, 327. (c) McGreal, E. P.; Martinez-Pomares, L.; Gordon, S. *Mol. Immunol.* **2004**, *41*, 1109. (d) Rabinovich, G. A.; Rubinstein, N.; Toscano, M. A. *Biochim. Biophys. Acta, General Subjects* **2002**, *1572*, 274.

(3) (a) Dougherty, T. J.; Gomer, C. J.; Henderson, B. W.; Jori, G.; Kessel, D.; Korbelik, M.; Moan, J.; Peng, Q. *J. Natl. Cancer Inst.* **1998**, *90*, 889. (b) Bonnett, R. *Chem. Soc. Rev.* **1995**, *24*, 19. (c) Klyashchitsky, B. A.; Nechaeva, I. S.; Ponomaryov, G. V. *J. Controlled Release* **1994**, *29*, 1.

(4) (a) Weis, W. I.; Drickamer, K. *Annu. Rev. Biochem.* **1996**, *65*, 441. (b) Drickamer, K. *Structure* **1997**, *5*, 465. (c) Sharma, V.; Surolia, A. *J. Mol. Biol.* **1997**, *267*, 433. (d) Elgavish, S.; Shaanan, B. *Trends Biochem. Sci.* **1998**, *22*, 462.

(5) (a) Gupta, N.; Narula, A.; Srivatava, P. S. *J. Plant Biochem. Biotechnol.* **2004**, *13*, 141. (b) Prasad, K. N.; Podder, U. S. *Indian J. Agric. Biochem.* **2004**, *17*, 81. (c) Bertrand, O.; Cochet, S.; Ctron, J. P. *J. Chromatogr., A* **1998**, *822*, 19. (d) Nomura, K.; Ashida, H.; Uemura, N.; Kushibe, S.; Ozaki, T.; Yoshida, M. *Phytochemistry* **1998**, *49*, 667. (e) Latha, V. L.; Rao, R. N.; Nadimpalli, S. K. *Protein Expression Purif.* **2006**, *45*, 296. (f) Padma, P.; Komath, S. S.; Nadimpalli, S. K.; Swamy, M. J. *Phytochemistry* **1999**, *50*, 363.

(6) (a) Loris, R.; Imberty, A.; Beeckmans, S.; Van, D. E.; Read, J. S.; Bouckaert, J.; De, G. H.; Buts, L.; Wyns, L. *J. Biol. Chem.* **2003**, *278*, 16297. (b) Svensson, C.; Teneberg, S.; Nilsson, C. L.; Kjellberg, A.; Schwarz, F. P.; Sharon, N.; Krengel, U. *J. Mol. Biol.* **2002**, *321*, 69. (c) Jeyaprakash, A. A.; Katiyar, S.; Swaminathan, C. P.; Sekar, K.; Surolia, A.; Vijayan, M. *J. Mol. Biol.* **2003**, *332*, 217−28. (d) Kulkarni, K. A.; Sinha, S.; Katiyar, S.; Surolia, A.; Vijayan, M.; Suguna, K. *FEBS Lett.* **2005**, *579*, 6775. (e) Liu, Y.; Misulovin, Z.; Bjorkman, P. J. *J. Mol. Biol.* **2001**, *305*, 481. (f) Sanders, D. A. R.; Moothoo, D. N.; Raftery, J.; Howard, A. J.; Helliwell, J. R.; Naismith, J. H. *J. Mol. Biol.* **2001**, *310*, 875. (g) Velloso, L. M.; Svensson, K.; Pettersson, R. F.; Lindqvist, Y. *J. Mol. Biol.* **2003**, *334*, 845. (h) Hamodrakas, S. J.; Kanellopoulos, P. N.; Pavlou, K.; Tucker, P. A. *J. Struct. Biol.* **1997**, *118*, 23.

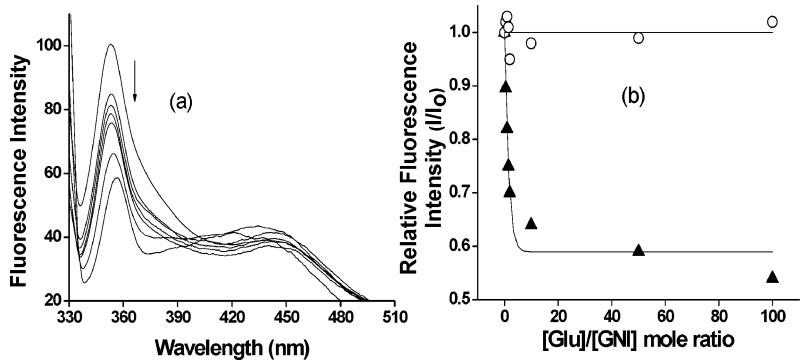

FIGURE 1. Fluorescence titration of **GNI** with Glu: (a) spectral traces at different additions of Glu; (b) plot of relative fluorescence intensity (I/I_o) vs [Glu]/[**GNI**] mole ratio. Open circles are for the 445 nm band and filled triangles are for the 355 nm band.

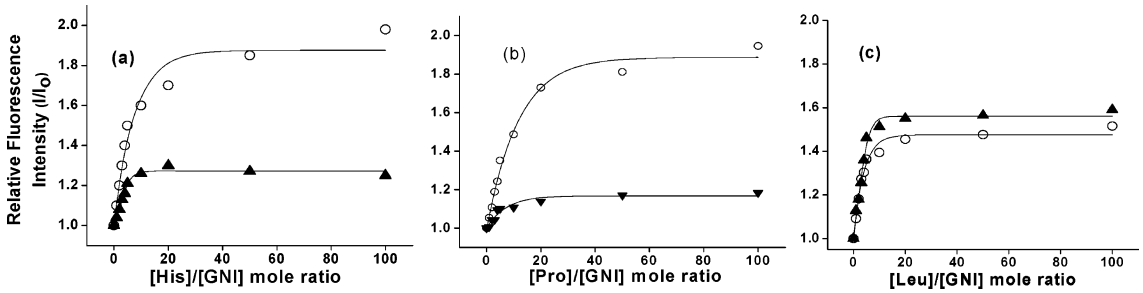

FIGURE 2. Plots of (I/I_o) vs mole ratio during the titration of **GNI** with amino acids: (a) His; (b) Pro; (c) Leu. Symbols have the same meanings as those in Figure 1.

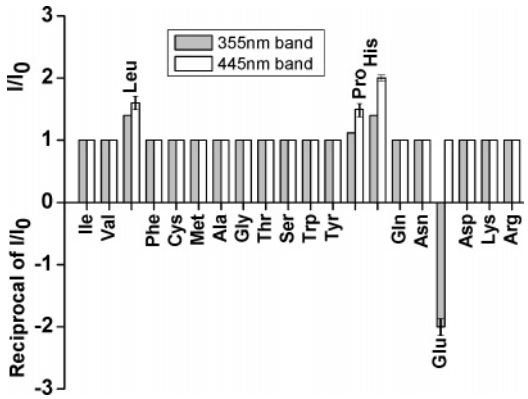

FIGURE 3. Histogram of (I/I_o) at saturation for the titration of **GNI** with amino acids. Positive values on the *y*-axis indicate enhancement fold in the fluorescence, and the negative values indicate quenching fold. All the titrations were repeated four times, and the variations obtained were indicated by error bars in the case of the interacting amino acids, viz., Glu, His, Pro, and Leu.

somewhat different in the case of Glu as compared to the other amino acids. This difference in the interaction has also been noted even in the absorption studies as reported in this paper.

The association constants (K_a) were calculated on the basis of the Benesi−Hildebrand equation, and the results are listed in Table 1. The K_a values suggest that the strength of the **GNI**···aa interaction follows a trend, viz., Leu > His > Pro based on the 455 nm band and Leu ≥ Glu ≫ His ≥ Pro based on the 355 nm band. The slopes of these plots yielded a 1:1 complex for Leu, His, and Pro and a 2:1 complex for Glu, where one Glu interacts with two **GNI**s.

Fluorescence Titration of GNA with Amino Acids. Although the titration of **GNI** with amino acids resulted either in enhancing or in quenching the fluorescence, the titrations with **GNA** resulted only in quenching the fluorescence in the case of the interacting amino acids (Supporting Information, S3). The titration of **GNA** with Ala, Cys, or Lys results in quenching the fluorescence intensity as the ratio of the added amino acid increases. The (I/I_0) plots clearly indicate a rapid quenching as shown in Figure 4, suggesting that these amino acids interact with **GNA**. However, all the remaining 17 amino acids showed no appreciable change (Figure 5). The extent of fluorescence quenching follows an order, Lys > Cys > Ala. Thus, the results clearly suggest that there exists a selective association between the **GNA** and the three amino acids, viz., Ala, Cys, and Lys, and this selectivity is different from that exhibited by **GNI**, as expected, owing to the presence of amine (−HN−CH_2−) in the former and imine (−C═N−) in the latter (Scheme 1). On going from the presence of imine (in **GNI**) to amine (in **GNA**), both the structural and the chemical functional differences emerge, and this leads to the differences in their recognition toward amino acids.

It was observed that the fluorescence emission quenching was too rapid to fit to the Benesi−Hildebrand equation, and hence Stern−Volmer analysis was employed to analyze the data. The occurrence of a nonlinear Stern−Volmer plot implied that a

TABLE 1. K_a and Slopes Obtained from Benesi−Hildebrand Plots in the Titration of GNI with the Interacting Amino Acids (aa)

	355 nm band		445 nm band	
aa	K_a (M^{-1})	slope	K_a (M^{-1})	slope
His	381 ± 30	nd[a]	10567 ± 2200	0.806 ± 0.01
Glu	28733 ± 3500	0.45 ± 0.05	nd[a]	nd[a]
Pro	nd[a]	nd[a]	1420 ± 160	1.06 ± 0.05
Leu	30911 ± 700	1.01 ± 0.01	22914 ± 520	1.02 ± 0.01

[a] nd: not determinable, as the changes observed in fluorescence intensity during the titration were not significant.

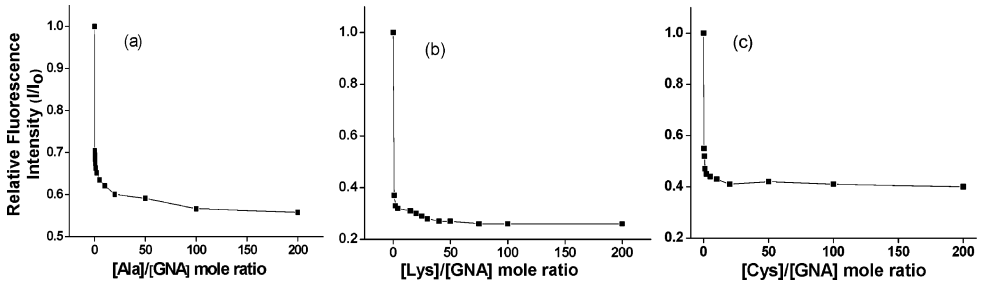

FIGURE 4. Plots of (I/I_o) vs amino acid mole ratio: (a) Ala; (b) Lys; (c) Cys.

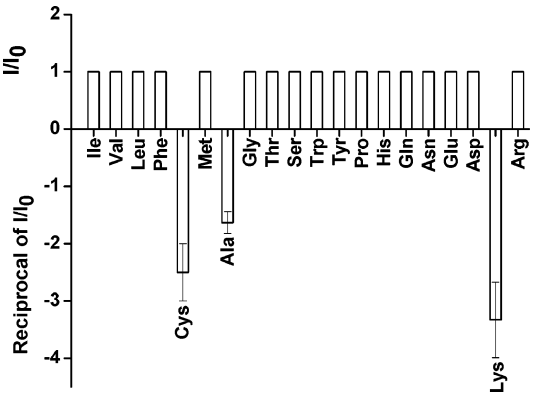

FIGURE 5. Histogram showing the relative fluorescence intensity at the saturation during the titration of **GNA** with different naturally occurring amino acids. For those amino acids that exhibit quenching, reciprocal (I/I_0) was shown which represents the number of times quenching occurs. The titrations were repeated four times, and the variations obtained were indicated by error bars in the case of the interacting amino acids, viz., Cys, Ala, and Lys.

proportion of the observed fluorescence is not susceptible to quenching. Hence, a modified Stern−Volmer expression was used

$$\frac{F_0}{F_0 - F} = \frac{1}{([\mathrm{Q}]K_{\mathrm{sv}}f_{\mathrm{a}})} + \frac{1}{f_{\mathrm{a}}}$$

where F_0 is the fluorescence intensity of the free **GNA**; F is the same in the presence of an amino acid (quencher); [Q] is the concentration of the quencher; K_{sv} is the Stern−Volmer constant; and f_a is the fraction of fluorescence that is susceptible to quenching. $K_{sv} = k_q\tau_0$, where the k_q is the quenching constant and τ_0 is the lifetime of the free ligand **GNA**. The corresponding modified Stern−Volmer plots are shown in Figure 6. All these were well fit with straight lines and hence support the assumption that the species were 1:1. From these plots, f_a and k_q were derived using the experimentally measured τ_0 for **GNA** being 4.92 ns based on the time-resolved fluorescence spectroscopy, and the data are listed in Table 2.

TABLE 2. Stern−Volmer Parameters (k_q and f_a) for the Titration of GNA with Interacting Amino Acids

aa	f_a	k_q ($M^{-1}s^{-1}$)
Lys	0.7 ± 0.03	1142 ± 150
Cys	0.58 ± 0.03	3831 ± 350
Ala	0.27 ± 0.02	949 ± 100

B. Absorption Spectral Studies. Absorption experiments were performed to confirm the binding of amino acids with **GNI** and **GNA**, and the details of the titration are given in the Experimental Section. The absorption bands observed in **GNI** and **GNA** were assigned upon comparison with the absorption spectra of naphthalene, β-naphthol, and 2-hydroxy-1-napthaldehyde (Supporting Information, S4). The bands observed at 220 and 300 nm in the case of **GNI** and those observed at 220, 277, and 334 nm were assignable to the naphthalene moiety and the OH attached to the C^{β} of the naphthalene moiety. The bands observed at 400 and 420 nm were distinctly present in **GNI** and not in **GNA** and hence are assignable to the imine function in **GNI**.

Absorption Titration of GNI with Amino Acids. Titration of **GNI** with Glu showed a gradual decrease followed by saturation of the absorbance of the 300 nm band as a function of added Glu, but no significant changes were observed in the 400 nm band. On the other hand, an increase in the absorbance was observed in both the bands in the case of the titration with other amino acids, viz., His, Leu, and Pro. Corresponding spectral traces were given in the Supporting Information (S5), and the absorbance plots are shown for all four cases in Figure 7. This behavior is analogous to that observed in the case of the fluorescence studies. The binding constants derived from the corresponding log plots are listed in Table 3 and were found to be in the order Glu > Pro > Leu based on the 300 nm band and His > Pro > Leu based on the 400 nm band.

From the absorption titrations, it was noted that the intensity of the 220 nm band decreases as the added [His] increases, as

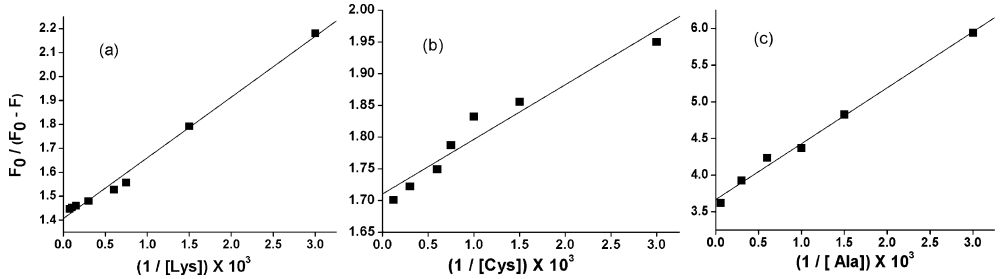

FIGURE 6. Modified Stern−Volmer plots for the interaction of **GNA** with Lys, Cys, and Ala. $F_0/(F_0 - F)$ is plotted against 1/[amino acid].

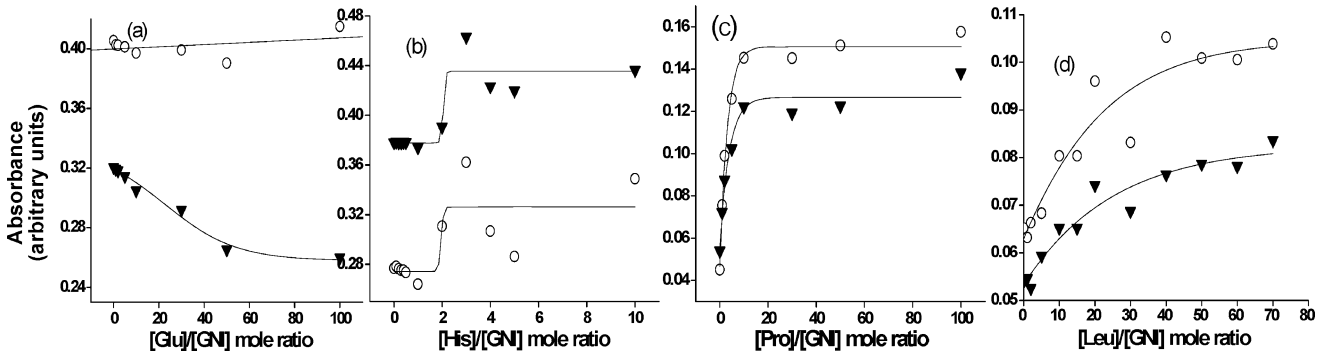

FIGURE 7. Absorbance of 300 nm (circles) and 400 nm (filled triangles) bands in the titration of **GNI** with amino acid: (a) Glu; (b) His; (c) Pro; and (d) Leu.

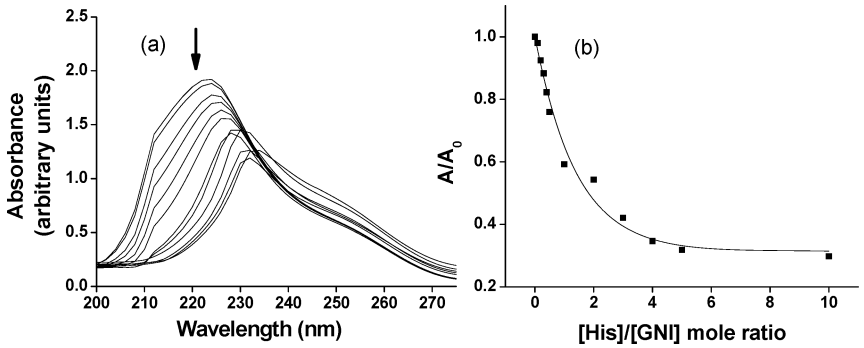

FIGURE 8. (a) Absorption spectral traces in the range 200−275 nm for the titration of **GNI** with His. (b) Relative absorbance of the titration shown in (a) as a function of [His]/[**GNI**] mole ratio.

TABLE 3. Association Constants (K_a) Derived from 300 and 400 nm Bands in the Absorption Spectra of the Titration of GNI with Interacting Amino Acids

	K_a (M^{-1})	
aa	300 nm band	400 nm band
Glu	35481 ± 3200	nd[a]
His	nd[a]	8317 ± 1100
Pro	5011 ± 700	3162 ± 400
Leu	1995 ± 200	1778 ± 150

[a] nd: not determinable, as the changes observed in OD during the titration were not significant.

shown in Figure 8a, and the plot shown in Figure 8b yields a K_a value of 38 018 M^{-1}. However, no significant change was observed in this band with the other three amino acids, viz., Glu, Pro, and Leu. Therefore, the change observed in the absorbance of this band could be a result of the interaction of the amino acid with the naphthyl moiety. Indeed, the computational calculations provided a long-range interaction between the imidazole nitrogen and skeletal carbons of the naphthyl moiety, as discussed later in this paper.

Absorption Titration of GNA with Amino Acids. Titration of **GNA** with Ala showed a gradual decrease followed by saturation in the absorbance of both the 277 and 334 nm bands. However, Cys and Lys exhibited an increase in the absorbance of both of the bands. Corresponding spectral traces were given in the Supporting Information (S6), and the absorbance plots are shown for all three cases in Figure 9. The changes in the absorbance follow a trend, Lys ≫ Cys ≥ Ala. The binding constants derived from the corresponding log plots are listed in Table 4.

Titration of a noninteracting amino acid, viz., Met, exhibited no significant change in the absorbance of any of the bands of either **GNI** or **GNA**. Thus, the absorption studies reported in this paper clearly demonstrate the binding selectivity of a particular amino acid with **GNI** or **GNA**.

C. Time-Resolved Fluorescence Spectroscopy. The fluorescence decay of **GNI** in water can be fitted to biexponential, yielding two lifetimes (τ_1 and τ_2) where the 9.06 ns has a higher contribution to the lifetime. The lifetime data for the titration of **GNI** with the interacting amino acids are presented in Table 5. Significant increases in the lifetimes were observed in the presence of amino acids, and they exhibited a trend, viz., Leu > His > Pro, synonymous with steady-state flouorescence results. Although the species with a lower lifetime is present in a high proportion in the case of Leu, it is the higher-lifetime species that is present in maximum proportion in the cases of His and Pro. On the other hand, **GNI** exhibited quenching of steady-state fluorescence in the presence of Glu and also exhibited a concomitant decrease in the lifetime of the species where both the species were present to almost an equal extent. Thus, the fluorescence lifetime studies clearly indicated a difference in the decay of the **GNI**···aa complexes from that of the simple **GNI**.

The fluorescence decay of **GNA** in MeOH can be fitted to a single exponential yielding a lifetime of 4.92 ns. As the medium is changed from MeOH to water, the lifetime increases to 5.18 ns (2:1 volume ratio of MeOH to H_2O) followed by 5.38 ns (1:2 volume ratio of MeOH to H_2O) and fits better to a biexponential decay. In a 1:29 volume ratio of MeOH to H_2O, the decay curve could be fitted to yield two species with lifetimes of 2.28 and 4.42 ns. This change is indicative of the dissociation of naphthyl−OH in water. In the titration of **GNA** with Ala, the lifetime decreases considerably as the ratio of Ala to **GNA** increases and approaches 3.98 ns at a 100:1 ratio. On

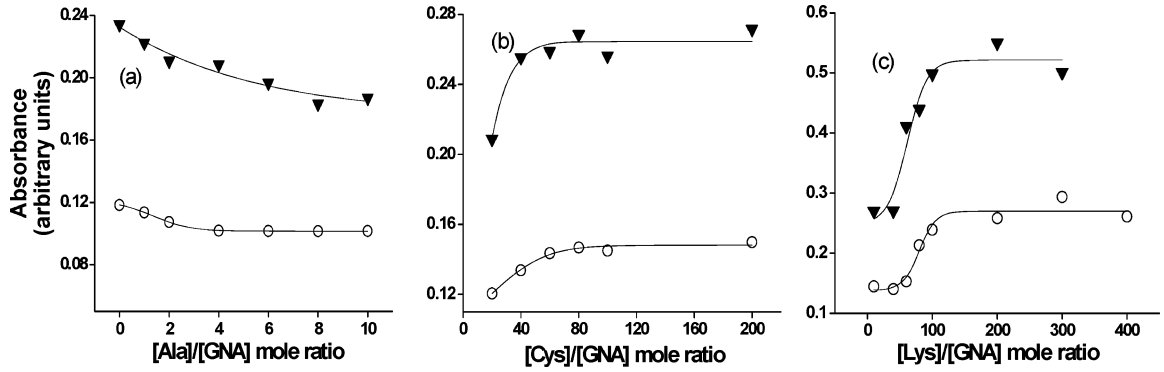

FIGURE 9. Absorbance of 277 nm (filled triangles) and 334 nm (circles) bands in the titration of **GNA** with amino acid: (a) Ala; (b) Cys; and (c) Lys.

TABLE 4. K_a Obtained for 277 and 334 nm Bands Based on the Absorption Spectra in the Titration of Interacting Amino Acids with GNA

	K_a (M^{-1})	
aa	277 nm band	334 nm band
Ala	6309 ± 700	nd[a]
Cys	1778 ± 250	5011 ± 350
Lys	3162 ± 300	2344 ± 250

[a] nd: not determinable, as the changes observed in OD during the titration were not significant.

TABLE 5. Fluorescence Lifetime Data for GNI···aa Systems[a]

system	τ_1 (ns)	τ_2 (ns)	$\chi^{2\,b}$
GNI (water)	0.70 (21%)	9.06 (79%)	1.195
GNI + Leu	2.26 (85%)	15.2 (15%)	1.087
GNI + His	1.48 (36%)	9.23 (64%)	1.250
GNI + Pro	1.29 (34%)	7.99 (66%)	1.321
GNI + Glu	0.44 (46.5)	5.46 (54%)	1.304

[a]The values given in brackets indicate the percent of species corresponding to that lifetime. [b]χ^2 represents goodness of fit.

the other hand, Lys and Cys did not exhibit any significant change in the lifetimes of **GNA**.

D. Electrospray Ionization Mass Spectral Studies. GNI···aa Complexes. An ESI mass spectrum of **GNI** shows abundant ions at *m*/*z* 334, 667, and 1000 corresponding to the protonated monomer, dimer, and trimer of **GNI**, respectively, as marked in Figure 10a. Mass spectra were also recorded for the reaction mixtures of **GNI** and amino acids. All these spectra show the $[M + H]^+$ ion of amino acid and **GNI**. In addition to the $[M + H]^+$ ions, the spectra also include the ions at *m*/*z* 465, 489, and 449 corresponding to the 1:1 complex of **GNI** with Leu, His, and Pro, respectively (Figure 10b−d). However, the peak observed at *m*/*z* 813 in the case of Glu titration is assignable to a 2:1 complex formed between **GNI** and Glu (Figure 10e). Thus, the mass spectral data supports the results obtained from the fluorescence studies.

GNA···aa Complexes. Unlike in the case of **GNI**, **GNA** failed to give the $[M + H]^+$ ion in the ESI experiments and rather gives an abundant peak at *m*/*z* of 157 corresponding to the naphthyl moiety that is formed by the cleavage of the −C−N− amine bond. Another ion with low abundance was observed at *m*/*z* 174 corresponding to the naphthyl−NH_3^+ moiety that is formed by the cleavage of the C_1(carb)−N bond. Although the ESI spectrum of Lys titration with **GNA** showed a peak at *m*/*z* 304 (157 + 147, i.e., naphthyl fragment + Lys), that of the Ala (MW 89) exhibited a peak at 263 (174 + 89, i.e., naphthyl−NH_3^+ moiety + Ala), indicating the formation of a 1:1 species between **GNA** and the amino acid. The mass spectra obtained for the titration mixtures of amino acids with **GNA** were given in the Supporting Information (S7).

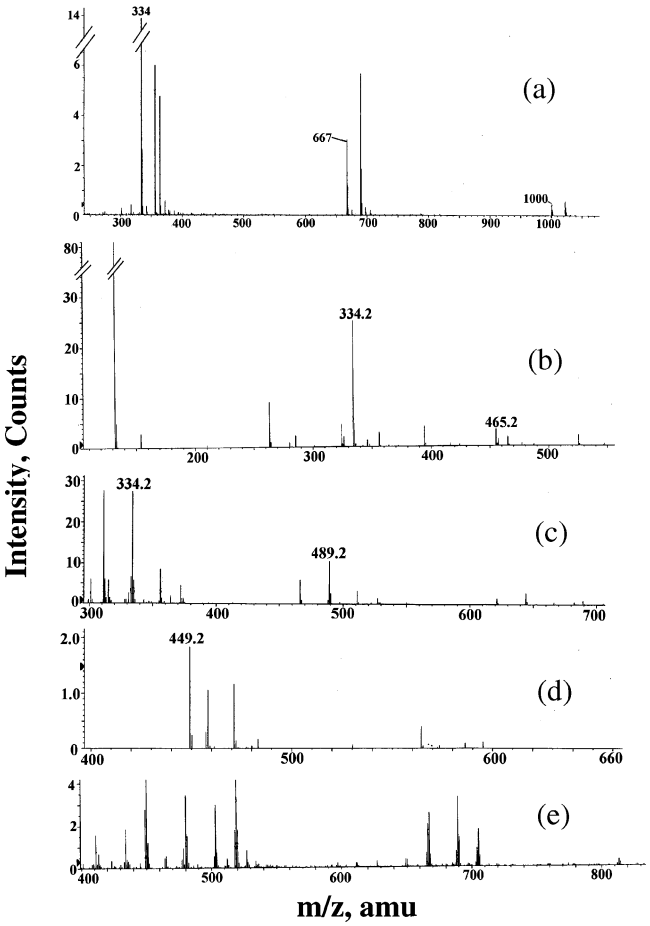

FIGURE 10. ESI mass spectra of (a) **GNI** (*m*/*z* = 334 $[M + H]^+$, 667 $[2M + H]^+$), 1000 $[3M + H]^+$); (b) **GNI···**Leu (1:1 at 465); (c) **GNI···**His (1:1 at 489); (d) **GNI···**Pro (1:1 at 449); (e) **GNI···**Glu···**GNI** (813).

E. Computational Modeling Studies of the Interaction of GNI and GNA with Amino Acids. Whether a particular amino acid among the naturally occurring ones interacts with **GNI**/**GNA** has been identified on the basis of fluorescence and absorption titration studies. The ratio of the complex formed between the carbohydrate derivative and the amino acid has

TABLE 6. Energies Obtained at Various Theories and Basis Sets of Calculations for GNI···aa Complexes

theory/basis set	aa	E_c (au)	E_{aa}* (au)	E_{GNI}* (au)	ΔE_s^p (kcal/mol)	ΔE_s^q (kcal/mol)	ΔE_s^r (kcal/mol)
PM3	Pro	−0.4897188	−0.1603063	−0.3249927	−2.8		
	Leu	−0.5083708	−0.1821584	−0.3087684	−10.9		
	His	−0.4317982	−0.1001654	−0.3250396	−4.1		
	Glu#	−0.9091673	−0.3016028	−0.3027776	−0.1		
				−0.3046010			
HF/3-21g	Pro	−1548.572810	−396.5422555	−1151.990046	−25.4		
	Leu	−1588.548620	−436.5207011	−1151.961252	−41.8		
	His	−1694.501016	−542.4658042	−1151.985266	−31.3		
	Glu	−2849.499224	−545.452826	−1151.991956	−45.0		
				−1151.982736			
B3LYP/3-21g	Pro	−1557.908234	−398.9423409	−1158.907427	−36.7		
	Leu	−1598.237086	−439.2437758	−1158.908178	−53.4		
	His	−1704.689125	−545.7117657	−1158.908178	−43.4		
	Glu	−2866.494713	−548.5554430	−1158.913280	−79.5		
				−1158.899298			
B3LYP/6-311g	Pro	−1566.439449	−401.1302801	−1165.284342	−15.6	−7.8	−8.0
	Leu	−1606.991102	−441.6556082	−1165.285594	−31.3	−23.1	−19.9
	His	−1714.041436	−548.7189270	−1165.281281	−25.9	−17.8	−15.1
	Glu	−2882.209291	−551.5876602	−1165.276336	−42.5	−25.3	−23.5
				−1165.277522			

* Single-point energy calculation of that moiety as taken from the optimized complex. #There are two **GNI** units for each Glu because the complex formed is 2:1. *p*Both the optimizations and single-point calculation in B3LYP/6-311G. *q*Optimizations in B3LYP/6-311G and single-point calculations in B3LYP/6-31+G(2d,2p). *r*Both the optimizations and single-point calculations in B3LYP/6-31+G(2d,2p).

TABLE 7. Energies Obtained at Various Theories and Basis Sets of Calculations for GNA···aa Complexes

theory/basis set	aa	E_c (au)	E_{aa}* (au)	E_{GNA}* (au)	ΔE_s^p (kcal/mol)	ΔE_s^q (kcal/mol)	ΔE_s^r (kcal/mol)
PM3	Ala	−0.5097037	−0.1549692	−0.3427969	−7.5		
	Cys	−0.4989198	−0.1419150	−0.3519648	−3.1		
	Lys	−0.5376265	−0.1759187	−0.3533305	−5.3		
HF/3-21g	Ala	−1473.281240	−320.0618100	−1153.137045	−51.7		
	Cys	−1868.811785	−715.6202512	−1153.157994	−21.0		
	Lys	−1644.448230	−491.2329172	−1153.154548	−38.1		
B3LYP/ 3-21g	Ala	−1482.107285	−321.9413370	−1160.072495	−58.6		
	Cys	−1878.346565	−718.1616621	−1160.098448	−54.2		
	Lys	−1654.455628	−494.2850140	−1160.107469	−39.6		
B3LYP/ 6-311g	Ala	−1490.256626	−323.7162677	−1166.470768	−43.7	−27.3	−24.4
	Cys	−1888.427421	−721.8963067	−1166.486485	−28.0	−21.0	−8.7
	Lys	−1663.526843	−497.0006997	−1166.491479	−21.8	−15.3	−18.4

* Single-point energy calculation of that moiety as taken from the optimized complex. *p*Both the optimizations and single-point calculation in B3LYP/6-311G. *q*Optimizations in B3LYP/6-311G and single-point calculations in B3LYP/6-31+G(2d,2p). *r*Both the optimizations and single-point calculations in B3LYP/6-31+G(2d,2p).

been derived on the basis of the titration data and was further confirmed on the basis of mass spectral studies. All the computational calculations were performed using Gaussian 98[7a] and/or Gaussian 03.[7b] Prior to assuming the initial guess model for computational calculations, the interactions present between the carbohydrates and the amino acids were examined by analyzing several crystal structures of lectin···carbohydrate complexes, and it was found that more than 50% of the interactions were indeed through −COOH and $-CONH_2$ moieties of Asp, Glu, Asn, and Gln. Further, it has been noted that the carbohydrate moiety mainly interacts through O4 and O6 and to some extent through O3.[7c] Therefore, the initial models for the complexes were generated by keeping all these factors in mind and were used for the geometry optimization initially at the semiempirical PM3 level of calculations. The resulting geometry output from these calculations always exhibited certain weak interactions between the **GNI** or **GNA** and the corresponding amino acid. The model obtained from the PM3 calculations was further optimized using ab initio HF/3-21G. The outcome of this calculation provided a better picture of the interactions present between the **GNI** or **GNA** and the amino acid. The outcome obtained at this stage was further optimized using hybrid density functional theory (DFT) with B3LYP/3-21G. The model obtained at this stage was finally optimized using B3LYP/6-311G. Thus, the calculations were carried out in a cascade fashion by going through PM3 → HF/3-21G → B3LYP/3-21G → B3LYP/6-311G. At every level of calculation, the stabilization energy of the complex formed (ΔE_s) was computed using the formula $\Delta E_s = E_c - E_{(\mathbf{GNI/GNA})} - E_{aa}$, where E_c is the total energy of the complex, $E_{(\mathbf{GNI/GNA})}$ is the energy of the glyco-conjugate, and E_{aa} is that of the amino acid, all taken at the same level of calculations. $E_{(\mathbf{GNI/GNA})}$ and E_{aa} were obtained by single-point calculations upon taking the corresponding moiety from the optimized complex. Energy data obtained at all these theories are shown in Tables 6 and 7 for **GNI** and **GNA** complexes, respectively (Supporting Information, S8). The data suggest that the complexation stabilities (ΔE_s^p) follow an order of PM3 < HF/3-21G < B3LYP/3-21G > B3LYP/6-311G. As the stabilization energies obtained at this stage were found to be higher than that expected based on the observed interactions, further computations were carried out using B3LYP/6-31+G(2d,2p) which takes care of the diffusion and polarization effects. Use of such functions yielded better

TABLE 8. Hydrogen-Bond Data for the GNI···aa Complexes at the B3LYP/6-31+G(2d,2p) Level of Calculations

complex	description of H-bonding	D···H (Å)	H···A (Å)	D···A (Å)	D···H···A (deg)
GNI···Glu (2:1)	C═O(Glu)···H−O−C2(carb) **GNI**-1	0.97	2.18	2.94	134.7
	N−H(Glu)···O−C2(carb) **GNI**-1	1.01	2.43	3.24	135.3
	C−O−H(side chain−Glu)···O−C4(carb) **GNI**-2	0.99	1.81	2.80	171.6
	C═O(side chain−Glu)···O−C6(carb) **GNI**-2	0.98	1.80	2.76	165.4
GNI···His (1:1)	C═O(His)···H−O−C3(carb)	0.97	1.81	2.76	163.5
	C−O−H(His)···O−C4(carb)	0.99	1.69	2.67	174.5
GNI···Leu (1:1)	C═O(Leu)···H−O−C6(carb)	0.98	1.80	2.78	175.57
	C−O−H(Leu)···O(napthyl)	1.01	1.60	2.60	176.0
GNI···Pro (1:1)	C−O(Pro)···H−O−C6(carb)	0.96	2.52	3.18	125.3
	C−O−H(Pro)···C4−O(carb)	0.98	1.91	2.82	153.1

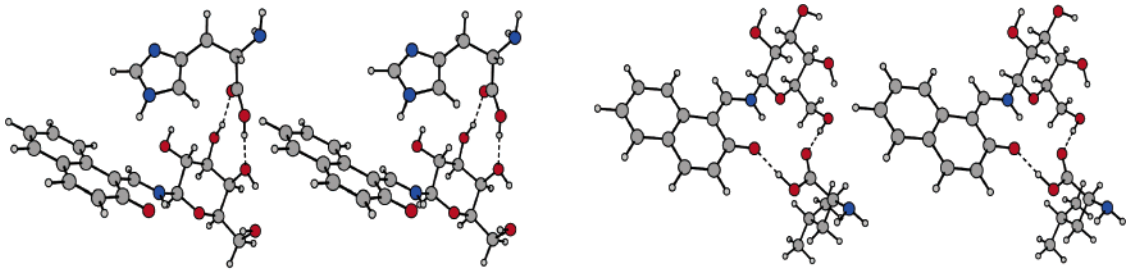

FIGURE 11. Stereoviews of the optimized structures [at B3YLP/6-31+G(2d,2p)] of the complexes formed between **GNI** and amino acids: (a) His and (b) Leu. Identification of atom type: C (gray); O (red); N (blue); H (small circle). The same labeling scheme was used in all the figures.

results in the case of carbohydrate systems as reported in the literature.[7d−g] The corresponding computations were carried out in two stages: (a) in the first stage, the stabilization energies (ΔE_s^q) were computed using the geometry obtained from B3LYP/6-311G and the single-point energy calculations carried out for individual components using B3LYP/6-31+G(2d,2p); (b) in the second stage, the complex stabilization energies (ΔE_s^r) were computed where both the optimization and the single-point energy calculations were performed using B3LYP/6-31+G(2d,2p).

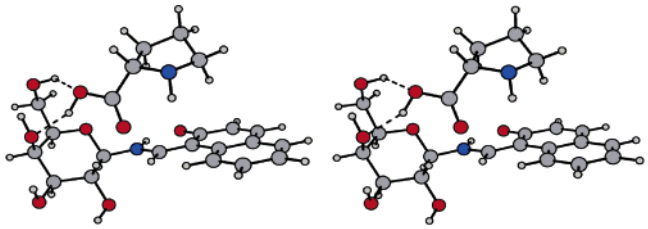

FIGURE 12. Stereoview of the optimized structure [at B3YLP/6-31+G(2d,2p)] of the complex formed between **GNI** and Pro.

GNI···aa Complexes. The calculations were carried out between **GNI** and His, Leu, or Pro as 1:1 complexes and with Glu as a 2:1 complex at all levels of theories mentioned earlier, and the corresponding formation (stabilization) energies of these complexes (ΔE_s^p, ΔE_s^q, and ΔE_s^r) are reported in Table 6. Different complexes of **GNI**···aa exhibited different hydrogen bond interactions where these interactions differ in their number, type, and strength, as can be noticed from the data listed in Table 8 for the structures obtained at B3LYP/6-31+G(2d,2p).

The complexes of **GNI**···His and **GNI**···Leu were mainly formed through the interaction of the carboxylic moiety of the amino acid with **GNI** but altogether in a different fashion, as can be seen from Figure 11. Thus, the **GNI**···His complex is stabilized through two hydrogen bond interactions formed between the carboxylic function of His and C3-OH and C4-OH moieties of the carbohydrate portion of the **GNI** to result in a nine-membered ring as shown in Figure 11a. In these two hydrogen bonds, although the −COOH group acts as both a donor and an acceptor, C3-OH acts as only a donor and C4-OH acts as only an acceptor. The imidazole moiety of His is placed right on the top of the naphthyl moiety where the distance between $N_{imidazole}$ and C_{imine}, C_1, C_8, and C_9 (of naphthyl) is

(7) (a) Frisch, M. J.; Trucks, G. W.; Schlegel, H. B.; Scuseria, G. E.; Robb, M. A.; Cheeseman, J. R.; Zakrzewski, V. G.; Montgomery, J. A., Jr.; Stratmann, R. E.; Burant, J. C.; Dapprich, S.; Millam, J. M.; Daniels, A. D.; Kudin, K. N.; Strain, M. C.; Farkas, O.; Tomasi, J.; Barone, V.; Cossi, M.; Cammi, R.; Mennucci, B.; Pomelli, C.; Adamo, C.; Clifford, S.; Ochterski, J.; Petersson, G. A.; Ayala, P. Y.; Cui, Q.; Morokuma, K.; Malick, D. K.; Rabuck, A. D.; Raghavachari, K.; Foresman, J. B.; Cioslowski, J.; Ortiz, J. V.; Stefanov, B. B.; Liu, G.; Liashenko, A.; Piskorz, P.; Komaromi, I.; Gomperts, R.; Martin, R. L.; Fox, D. J.; Keith, T.; Al-Laham, M. A.; Peng, C. Y.; Nanayakkara, A.; Gonzalez, C.; Challacombe, M.; Gill, P. M. W.; Johnson, B. G.; Chen, W.; Wong, M. W.; Andres, J. L.; Head-Gordon, M.; Replogle, E. S.; Pople, J. A. *Gaussian 98*, revision A.7; Gaussian, Inc.: Pittsburgh, PA, 1998. (b) Frisch, M. J.; Trucks, G. W.; Schlegel, H. B.; Scuseria, G. E.; Robb, M. A.; Cheeseman, J. R.; Montgomery, J. A., Jr.; Vreven, T.; Kudin, K. N.; Burant, J. C.; Millam, J. M.; Iyengar, S. S.; Tomasi, J.; Barone, V.; Mennucci, B.; Cossi, M.; Scalmani, G.; Rega, N.; Petersson, G. A.; Nakatsuji, H.; Hada, M.; Ehara, M.; Toyota, K.; Fukuda, R.; Hasegawa, J.; Ishida, M.; Nakajima, T.; Honda, Y.; Kitao, O.; Nakai, H.; Klene, M.; Li, X.; Knox, J. E.; Hratchian, H. P.; Cross, J. B.; Bakken, V.; Adamo, C.; Jaramillo, J.; Gomperts, R.; Stratmann, R. E.; Yazyev, O.; Austin, A. J.; Cammi, R.; Pomelli, C.; Ochterski, J. W.; Ayala, P. Y.; Morokuma, K.; Voth, G. A.; Salvador, P.; Dannenberg, J. J.; Zakrzewski, V. G.; Dapprich, S.; Daniels, A. D.; Strain, M. C.; Farkas, O.; Malick, D. K.; Rabuck, A. D.; Raghavachari, K.; Foresman, J. B.; Ortiz, J. V.; Cui, Q.; Baboul, A. G.; Clifford, S.; Cioslowski, J.; Stefanov, B. B.; Liu, G.; Liashenko, A.; Piskorz, P.; Komaromi, I.; Martin, R. L.; Fox, D. J.; Keith, T.; Al-Laham, M. A.; Peng, C. Y.; Nanayakkara, A.; Challacombe, M.; Gill, P. M. W.; Johnson, B.; Chen, W.; Wong, M. W.; Gonzalez, C.; Pople, J. A. *Gaussian 03*, revision C.02; Gaussian, Inc.: Wallingford, CT, 2004. (c) Prakash C. J.; Rao, C. P., unpublished results. (d) Barrows, S. E.; Dulles, F. J.; Cramer, C. J.; French, A. D.; Truhlar, D. G. *Carbohydr. Res.* **1995**, *276*, 219. (e) Csonka, G. I. *J. Mol. Struct.* (*Theochem*) **2002**, *584*, 1. (f) Lii, J.-H.; Ma, B.; Allinger, N. L. *J. Comput. Chem.* **1999**, *20*, 1593. (g) Allinger, N. L.; Schleyer, P. V. R. *J. Comput. Chem.* **1993**, *14*, 1.

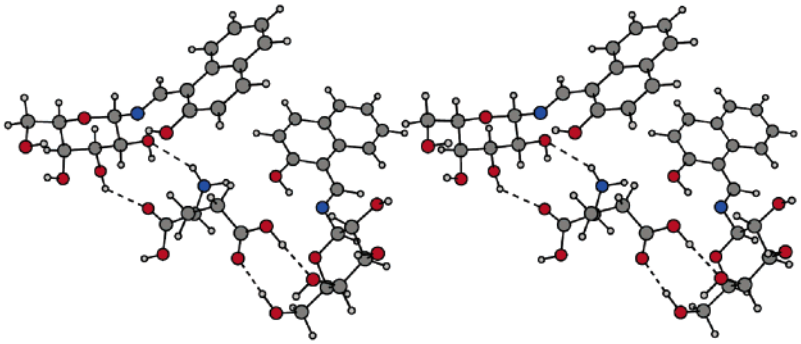

FIGURE 13. Stereoview of the optimized structure [at B3YLP/6-31+G(2d,2p)] of the 2:1 complex formed between **GNI** and Glu.

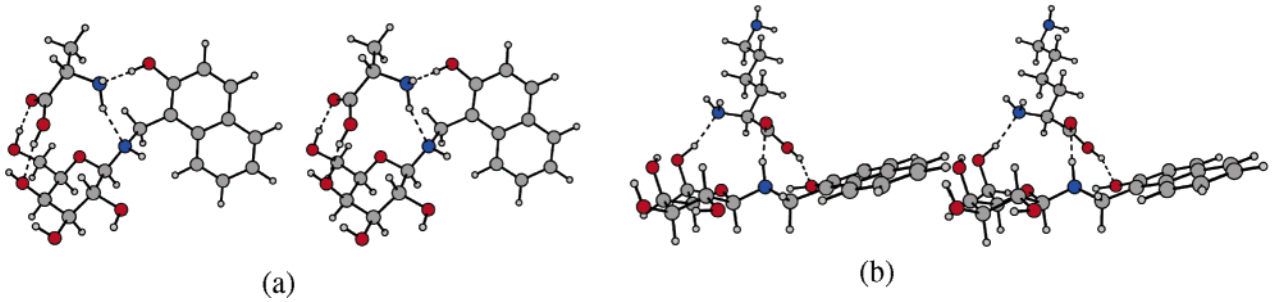

FIGURE 14. Stereoviews of the optimized structures [at B3YLP/6-31+G(2d,2p)] of the complexes formed between **GNA** and amino acids: (a) Ala and (b) Lys.

TABLE 9. Hydrogen-Bond Data for the GNA···Amino Acid Complexes at the B3LYP/6-31+G(2d,2p) Level of Calculations

complex	description of H-bonding	D···H (Å)	H···A (Å)	D···A (Å)	D···H···A (deg)
GNA···Ala (1:1)	C═O(Ala)···H−O−C6(carb)	0.98	1.77	2.74	169.2
	C−O−H(Ala)···O−C6−O(carb)	0.98	1.85	2.82	170.0
	N(Ala)···H−O(napthyl)	0.99	1.75	2.75	177.5
	N−H(Ala)···N(**GNA**)	1.02	2.11	3.07	154.7
GNA···Cys (1:1)	S(Cys)···H−O−C6(carb)	0.97	2.40	3.35	165.9
	C═O(Cys)···H−N(**GNA**)	1.01	2.16	3.12	158.1
	C^{β}−H···O_{naph}	1.09	2.54	3.59	161.9
GNA···Lys (1:1)	C═O(Lys)···H−N	1.01	2.48	3.19	126.7
	N(Lys)···H−O−C6	0.99	1.85	2.82	165.7
	C−O−H(Lys)···O(napthyl)	0.99	1.74	2.70	160.5

3.9 ± 0.4 Å. On the other hand, in the **GNI**···Leu complex, the −COOH group of Leu is also involved in two H-bonds but is extended to the C6-OH moiety of the carbohydrate (C═O_{Leu}···H−O−C6) and the naphthylic-OH (C−O−H_{Leu}···O_{naph}) resulting in a 16-membered H-bonded network as shown in Figure 11b.

Unlike in the cases of **GNI**···His and **GNI**···Leu, in the **GNI**···Pro complex, the −COOH group of Pro interacts only through its C═O and not through its −OH. Thus, among the 1:1 complexes of **GNI**···aa, the combination with Pro results in a weak complex interacting through two H-bonds extending between the OH group of the carboxylic moiety and C4-OH and C6-OH groups in a cyclic fashion to result in a six-membered H-bond network as shown in Figure 12. Thus, among these three 1:1 complexes, the ΔE_s^r follows the order **GNI**··· Leu > **GNI**···His > **GNI**···Pro, and this trend was also reflected in the K_a obtained from fluorescence data.

In the case of the **GNI**···Glu complex, the side chain −COOH of Glu interacts with one **GNI** through two H-bonds extended from the C4-OH and C6-OH groups. The second **GNI** interacts rather weakly through the C2-OH moiety with the C═O and amine function of Glu. All these interactions can be viewed from Figure 13. Thus, Glu moves toward the hydrophilic carbohydrate moiety to a greater extent. It is evident from the crystal structures of lectin···carbohydrate complexes that the −COOH side chain of Glu and Asp interacts with the carbohydrate by using one or both of its oxygen centers similar to that found in the present case.[6a,c]

GNA···aa Complexes. The H-bond interactions found between **GNA** and the interacting amino acids were listed in Table 9. In the complexes of **GNA**···Ala and **GNA**·····Lys, both the C^{α}−NH_2 and the −COOH moieties of Ala and Lys interact with **GNA**, but differently, as can be seen from Figure 14. The NH_2 of Ala interacts with the naphthylic-OH and the amine

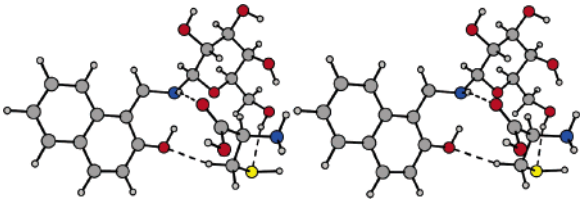

FIGURE 15. Stereoview of the optimized structure [at B3YLP/6-31+G(2d,2p)] of the complex of **GNA** and Cys.

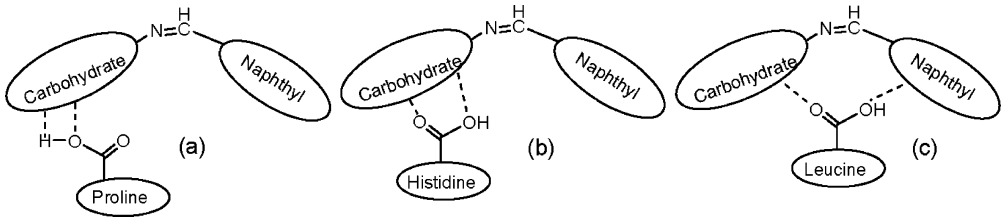

FIGURE 16. Schematic representation of the interactions present in the 1:1 complexes of **GNI** with (a) Pro, (b) His, and (c) Leu.

nitrogen of **GNA** to result in an eight-membered ring possessing $N-H_{Ala}\cdots N_{\mathbf{GNA}}$ and $O-H_{naph}\cdots N_{Ala}$. The −COOH of Ala interacts with C6-OH to result in a six-membered ring possessing $C6-O-H\cdots O{=}C_{Ala}$ and $C6-O\cdots H-O-C_{Ala}$ interactions. On the other hand, the **GNA**···Lys complex is stabilized through three hydrogen bonds (Figure 14b) resulting in 10- and 12-membered rings, viz., $N-H_{\mathbf{GNA}}\cdots O{=}C_{Lys}$, $H_2N_{Lys}\cdots H-O-C6$, and $C-OH_{Lys}\cdots O_{naph}$. Thus, the **GNA** acts as a H-donor for two H-bonds and as an acceptor for one.

In the complex of **GNA**···Cys, the amino acid interacts through its −COOH, −SH, and $C^{\beta}-H$ and forms three weak H-bonds with **GNA**, viz., $C{=}O_{Cys}\cdots H-N_{\mathbf{GNA}}$, $S_{Cys}\cdots H-O-C6_{\mathbf{GNA}}$, and $C^{\beta}-H\cdots O_{naph}$, as can be seen from Figure 15.

Carbohydrate Ring Conformation. In the case of **GNI** and its amino acid complexes, the carbohydrate moiety was found to be in $^4C_1$ chair conformation based on Cremer−Pople parameters[8] where the θ value is close to 0° but varies from 3.7 to 9.9°. In the case of **GNA** and its amino acid complexes, this angle varies from 2.1 to 25.4° indicating a higher puckering of the carbohydrate moiety in **GNA** complexes as compared to the **GNI** complexes. All the corresponding data were given in the Supporting Information (S9).

Relative Orientation of the Carbohydrate and Naphthyl Moieties. In free **GNI**, the average plane of the carbohydrate makes an obtuse angle with respect to the naphthyl plane where the distance between C6-O and O_{phen} is about 5.92 Å, and in its complexes of amino acids, the distance varies in the range 5.5−6.9 Å indicating direct access for the amino acid to interact with **GNI**. On the other hand, in free **GNA**, the average plane of the carbohydrate makes an acute angle, where the C6-O to O_{phen} distance is only 2.85 Å, and in its amino acid complexes, this distance varies in the range 5.5−7.3 Å to provide access to the amino acid for the interaction. Thus, the angle goes from acute to obtuse upon going from free **GNA** to its amino acid complexes.

The inclination of the average plane of the carbohydrate moiety with respect to the naphthyl plane increases in the order **GNI** ≤ **GNI**···Pro < **GNI**···His < **GNI**···Leu < **GNI**···Glu, wherein it approaches a perpendicular fashion in the case of the **GNI**···Glu complex. This can be gauged from the dihedral angle $C_N-N-C1_{carb}-C2_{carb}$ or $C_N-N-C1_{carb}-O_{carb}$ (Supporting Information, S9).

Positioning of N with Respect to the Naphthyl Plane. Although the nitrogen in **GNI** and its complexes is in the plane of the naphthyl moiety as expected, it deviates from this plane in the case of **GNA** by 1.008 Å as the $-HC{=}N-$ present in **GNI** is reduced to $-H_2C-NH-$. The deviation of N from the naphthyl plane is higher in the case of the **GNA**···Ala complex (1.46 Å) and lower in the cases of **GNA**···Cys (1.04 Å) and **GNA**···Lys (0.82 Å) when compared to **GNA**. The dihedral angle about the $-C{=}N-$ bond is very close to 180° (*trans*-imine) in the case of **GNI** and its aa complexes. On the other hand, the dihedral angle about −C−N− in **GNA** and its amino acid complexes substantially deviates from 180°. The deviation is 83° in the case of simple **GNA**, and the deviations are 15°, 28°, and 15°, respectively, in the cases of the **GNA**···Lys, **GNA**···Ala, and **GNA**···Cys complexes, suggesting that in the presence of amino acids −C−N− comes into the plane of the naphthyl ring.

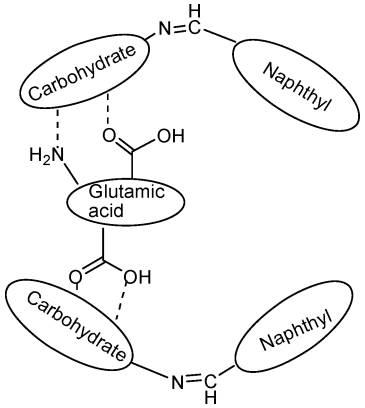

FIGURE 17. Schematic representation of the interactions present in the 2:1 complexes of **GNI** with Glu.

Conclusions and Correlations

In the 1:1 complexes of **GNI**···aa, the −COOH group of the amino acid primarily interacts with the carbohydrate moiety through either one or both of its oxygens (Figure 16a,b) or spans between both the carbohydrate and naphthyl units (Figure 16c). The imine nitrogen is not involved in any interaction in the complexes.

A similar trend in the interaction of the −COOH group toward the carbohydrate moiety continues to be present even in the 2:1 complex of **GNI** and Glu where both the C^{α} and C^{δ} carboxylic groups of Glu were involved in such interactions as shown in Figure 17. Thus, the −COOH moiety of amino acids exhibits high affinity toward carbohydrate in the imine-linked system, viz., **GNI**. Similar interactions were noted in the literature at the active site of α-galactosidase isolated from rice, where the substrate galactose interacts through the −COOH group of three different aspartate moieties.[9] Even the interactions of the substrate, *N*-acetylgalactose, with the enzyme, *N*-acetylgalactosaminidase, isolated from chicken were found to be the same.[10]Also noted from the crystal structures of lectin−carbohydrate complexes is the involvement of Glu and Asp in

(8) Cremer, D.; Pople, J. A. *J. Am. Chem. Soc.* **1975**, *97*, 1354.

(9) Zui, F.; Satoshi, K.; Mitsuru, M.; Hideyuki, K.; Hiroshi, M. *J. Biol. Chem.* **2003**, *278*, 20313.

(10) Garman, S. C.; Hannick, L. Z. A.; Garboczi, D. N. *Structure* **2002**, *10*, 425.

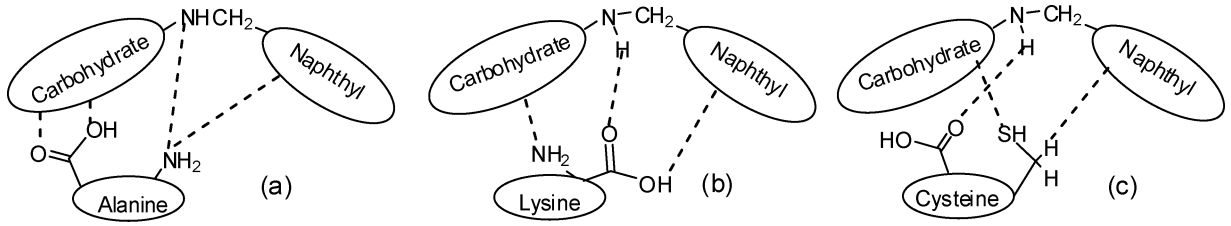

FIGURE 18. Schematic representation of the interactions present in the 1:1 complexes of **GNA** with (a) Ala, (b) Lys, and (c) Cys.

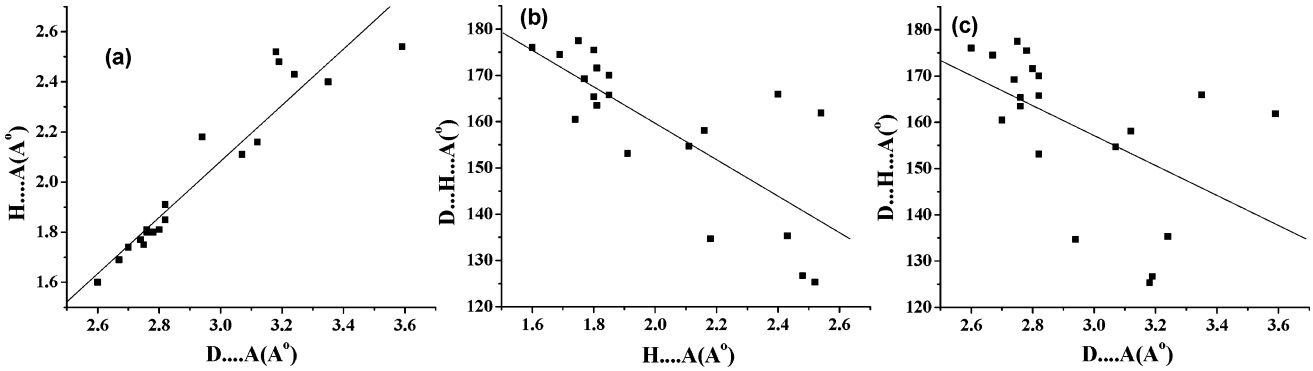

FIGURE 19. H-bond data correlations of the amino acid complexes of **GNI** and **GNA**: (a) D···A and H···A; (b) H···A vs D−H···A; (c) D···A vs D−H···A.

the interaction with carbohydrate.[7c] Of course, even the side chains of Asn and Ser/Thr were also involved in the lectin−carbohydrate interactions, besides the involvement of the peptide unit. In some cases, Phe and Tyr extended hydrophobic interactions using their aromatic portions.[6]

On the other hand, in the case of **GNA**···aa complexes, the amino acid moiety interacts with both the units of **GNA** as shown in Figure 18. The interacting amino acids do not exhibit any specificity in their binding toward either unit of **GNA** as can be noticed from this figure. Unlike **GNI**···aa complexes, those of **GNA** exhibit interactions through the amine nitrogen in all its complexes. Thus, it is the carboxylic group of the amino acid that exhibits high affinity toward the carbohydrate moiety in **GNI** complexes but not in **GNA**, owing to the changes in their molecular geometries. On the other hand, the nitrogen center extends interaction with the amino acid in the case of **GNA** complexes and not in the **GNI** complexes. The involvement of the nitrogen center in the interactions could be a possible reason for the loss of the specificity of the carbohydrate moiety toward the carboxylic group of the amino acid in the case of **GNA** as compared to **GNI** in their complexes.

The hydrogen bond data obtained from the computational calculations at the B3LYP/6-31+G(2d,2p) level (Tables 8 and 9) exhibited excellent linear correlation between D···A and H···A distances and fairly linear correlations among H···A vs the D−H···A angle and D···A vs the D−H···A angle as shown in Figure 19.

The stabilization energies of all these complexes in their optimized geometry [B3LYP/6-31+G(2d,2p)] were estimated using the plot given in the literature for H···A vs binding energy.[14] These estimated energies were compared with the computationally obtained ones (Tables 6 and 7; Supporting Information, S10), and a fairly linear correlation was found, as shown in Figure 20. The H-bond energies found in the case of the **GNI**/**GNA**···aa complexes suggest that these are primarily moderate H-bonds.

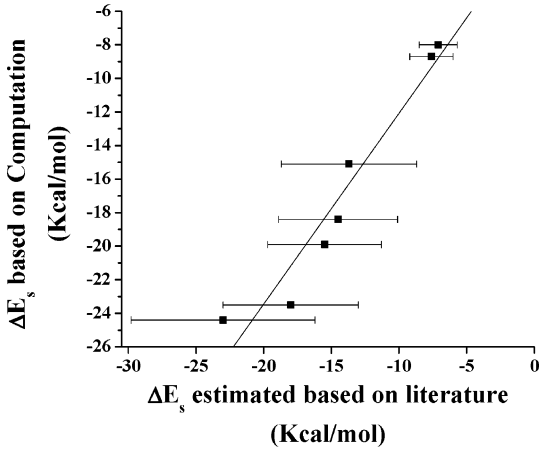

FIGURE 20. Plot of ΔE_s estimated using the literature (ref 14) vs ΔE_s^r obtained from the computation of all **GNI**/**GNA**···aa complexes.

The characteristics developed on the basis of emission and absorption spectral studies of the interaction of **GNI** and **GNA** with amino acids reported in this paper would be of great advantage in the detection and evaluation of amino acids in proteins, particularly those present at C- and N-terminal regions. Specifically, **GNI** would be well suited to detect Pro, His, Leu, and Glu present at the C-terminal region and perhaps Glu present in the interior of the oligo- and polypeptides over its counterpart, **GNA**. We have recently demonstrated the utility of **GNI** in recognizing Cu(II) in HEPES buffer, whereas **GNA** is ineffective under the same experimental conditions.[11] This paper, thus, certainly evokes interest in understanding carbohydrate···aa interactions of the synthetic carbohydrate analogues in the context of lectin···carbohydrate and glycosidase···substrate interactions.

(11) Singhal, N. K.; Ramanujam, B.; Mariappanadar, V.; Rao, C. P. *Org. Lett.* **2006**, *8*, 3525.

Experimental Section

D-Galactose (G) and 2-hydroxy-1-naphthaldehyde were procured from a commercial source. 2-Hydroxy-1-aminomethyl naphthalene was synthesized in the lab to make **GNA**. **G-NH$_2$**, **GNI** and **GNA** were synthesized and characterized as given below. All the solvents used were of AR grade and dried using standard procedures immediately before use.

Synthesis and Characterization of G-NH$_2$ (β-D-Galactopyranosyl-C-1-deoxy-C-1-amine). Through a chilled (using an ice−salt mixture) suspension of dried galactose (10 g) in methanol was bubbled dry ammonia gas for about 8−9 h. Then the reaction mixture was further stirred under an ammonical atmosphere for an additional 24 h at room temperature. After 3−4 days of refrigeration at 4 °C, a solid product was formed which was then isolated through filtration, and the residue was washed with methanol. Filtrate was washed and kept in a refrigerator to obtain a second crop of product (3.95 g, 39.5%). IR (KBr): 3373(b) $\upsilon_{(O-H)}$ and $\upsilon_{(N-H)}$, 2920(S) and 2910(S) $\upsilon_{(C-H)}$, 1611(S) $\delta_{(N-H)}$ cm^{-1}. ^{1}H NMR (DMSO-d_6): 2.36 (S, 2H, NH$_2$), 2.86−2.97 (m, H, C2-H), 3.03−3.31 (m, 4H, C3-H, C4-H, C6-H), 3.88 (d, H, $^3J_{C1-H-C2-H}$ = 8.4 Hz, C1-H), 3.95−4.00 (m, H, 5H), 4.72−5.63 (m, 4H, C2-OH, C3-OH, C4-OH, C6-OH) ppm. ^{13}C NMR (DMSO-d_6): δ 92.65 (C1), 68.84−70.40 (C3−C6), 60.67(*C*2) ppm. FABMS: *m*/*z* 180 ([M + H]$^+$, 90%), 179 ([M$^+$], 30%). Anal. calcd for $C_{17}H_{19}O_6N$: C, 40.00; H, 7.32; N, 7.83. Found: C, 39.38; H, 6.82; N, 7.62.

Synthesis and Characterization of GNI. To a suspension of **G-NH$_2$** (3.584 g, 20.02 mmol) in ethanol (45 mL) was added β-hydroxy napthaldehyde (3.612 g, 20.88 mmol), and the reaction mixture was allowed to reflux for 6 h. During the course of the reaction, a yellow solid was formed. The reaction mixture was allowed to cool to room temperature and was left as such overnight. Some more solid was formed which was then separated by filtration, washed with a small portion of methanol followed by petroleum ether, and dried under a vacuum. Product yield: 4.91 g (74%). IR (KBr): 3394(b) $\upsilon_{(O-H)}$ and $\upsilon_{(N-H)}$, 2938(S), 2935(S), and 2920(S) $\upsilon_{(C-H)}$, 1631(S) $\delta_{(CH=N)}$ cm^{-1}. ^{1}H NMR (DMSO-d_6): 3.12−3.57 (m, 6H, C2-H, C3-H, C-4H, C6-H), 3.72−3.75 (m, H, C5-H), 4.36−5.38 (m, 4H, C2-OH, C3-OH, C-4OH, C6-OH), 4.62 (d, H, $^3J_{C1-H-C2-H}$ = 11.02 Hz, C1-H), 6.77−7.81 (m, 6H, Ar−H), 8.11 (S, H, CH=N), 14.21 (S, H, Phenol-OH) ppm. ^{13}C NMR (DMSO-d_6): δ 91.10 (C1), 60.68−77.76 (C2−C6), 106.20−137.52 (Ar-10C), 158.10 (CH=N) ppm. FABMS: *m*/*z* 334 ([M + H]$^+$, 70%), 333 ([M$^+$], 40%). Anal. calcd for $C_{17}H_{19}O_6N$: C, 61.32; H, 5.72; N, 4.21. Found: C, 61.22; H, 6.00; N, 3.94.

Synthesis and Characterization of GNA. Dried galactose (**G**, 1.804 g, 10.02 mmol) and 1-methylamino-2-naphthol (1.782 g, 10.3 mmol) were suspended in 25 mL of ethanol. The reaction mixture was stirred for 24 h at room temperature followed by reflux for 8 h. The solid obtained was separated by filtration and dried under a vacuum. Product yield: 2.20 g (66%). IR (KBr): 3394(S) $\upsilon_{(O-H)}$ and $\upsilon_{(N-H)}$, 3208(S), 3027(S), and 2930(S) $\upsilon_{(C-H)}$, 1628(S) $\delta_{(CH-N)}$ cm^{-1}. ^{1}H NMR (DMSO-d_6): 3.36−3.70 (m, 6H, C2-H, C3-H, C-4H, C6-H), 3.74−3.79 (m, H, C5-H), 4.33−4.92 (m, 4H, C2-OH, C3-OH, C-4OH, C6-OH), 4.39−4.41 (S, 2H, nap-CH$_2$), 4.92 (S, H, C1-H), 6.16 (S, H, N−H), 7.30−8.13 (m, 6H, Ar−H) ppm. ^{13}C NMR (DMSO-d_6): δ 32.81 (nap-CH2), 68.85−79.76 (C2−C6), 110.97−154.52 (Ar-10C) ppm. FABMS: *m*/*z* ([M − 3]$^+$, 30%), 332. Anal. calcd for $C_{17}H_{19}O_6N$: C, 60.89; H, 6.32; N, 4.21. Found: C, 60.52; H, 6.56; N, 3.96.

Fluorescence Studies. To prepare the bulk solutions, **GNI** and **GNA** were initially dissolved in about 1 mL of DMSO followed by diluting with MeOH to a 10 mL solution to give concentrations of 10^{-3} and 10^{-4} M, respectively. The bulk solutions of the amino acids were made in deionized water to give a 10^{-3} M concentration. All the fluorescence studies were carried out on a Perkin-Elmer LS55 at 320 nm excitation, and the emissions were measured in the range 330−500/450 nm using 3 mL solutions filled in 1 cm quartz cells. Amino acid titrations were carried out by maintaining the final [**GNI**] at 6.67 μM and [**GNA**] at 1.67 μM with the addition of varying volumes of amino acid bulk solution to result in varying amino acid to ligand mole ratios and by maintaining a solution volume of 3 mL at each titration where the requisite dilution was carried out using MeOH. All the amino acid titrations were repeated at least three to four times.

Absorption Studies. To prepare the bulk solutions, **GNI** and **GNA** were initially dissolved in about 1 mL of DMSO followed by diluting with MeOH to a 10 mL solution to give concentrations of 10^{-2} and 10^{-3} M, respectively, i.e., the bulk solutions whose concentrations are 10-fold higher than those prepared for the fluorescence studies. The bulk solutions of the amino acids were made in deionized water both at 10^{-2} and 10^{-3} M. All the absorption studies were carried out on Jasco V-570, and the spectra were measured in the 200−500 nm region using the solutions filled in 1 cm quartz cells by maintaining the final [**GNI**] at 0.25 mM and [**GNA**] at 0.025 mM in a total solution volume of 2 mL achieved by diluting with MeOH. Before the dilution, the amino acid solutions were added to give varying amino acid to ligand mole ratios similar to that mentioned in the fluorescence studies. All the amino acid titrations were repeated at least two to three times.

Computational Studies. The structures of galactosyl derivatives and amino acids, viz., **GNI**, **GNA**, Pro, Leu, Glu, His, Ala, Cys, and Lys, were generated using Gaussview V.3.09, and their optimized structures were obtained using Gaussian 98 and/or Gaussian 03. Structures were first optimized using the semiempirical PM3 level of calculation to obtain low-energy starting structures, which were then geometry optimized using the HF/3-21G, B3LYP/3-21G, B3LYP/6-311G, and B3LYP/6-31+G(2d,2p) level of calculations in a cascade fashion where the input for the higher level of calculation is the output of the previous level. The above methodology was also used to model the complexes resulting from the interaction of galactosyl derivatives with the amino acids. In the initial input, the amino acid was placed at a noninteracting distance (more than 3 Å) from the galactosyl derivative.

Mass Spectrometry. ESI spectra were recorded for reaction mixtures of **GNI** and **GNA** with amino acids using a QSTAR XL mass spectrometer. The concentrations of the ligands were kept constant at 10^{-4} M in the final solution, and two samples corresponding to titration after the addition of 5 and 10 equiv of amino acids were prepared and analyzed.

Time-Resolved Fluorescence Measurements. Time-resolved data frequently contain more information than is available from the steady-state data. Time-resolved fluorescence experiments were performed with a time-domain fluorescence spectrometer model 199 which uses a gated hydrogen discharge lamp as the excitation source and an EG & G ORTEC single-photon-counting (SPC) data acquisition system, interfaced with an LSI-11/23 computer. The observed fluorescence decay function $F(t)$ was a convolution of the true fluorescence decay function $G(t)$ [$G(t) = \Sigma_i B_i \exp(-t/\tau_i)$, where B_i is the pre-exponential factor and τ_i is the fluorescence lifetime for the ith component] and the instrument response function $I(t)$ and was analyzed by using an appropriate reconvolution program employing a nonlinear iterative least-squares fit method. The mono- or multiexponential behavior of the true decay associated with the observed fluorescence decay function and the corresponding computer fit was evaluated by the minimum reduced χ^2 value as well as by the distribution of the weighted residuals among the data channels and the Durbin−Watson parameter.[12] The time resolution of the SPC unit, determined by Zimmermann's method,[13] was found to be ca. 100 ps.

(12) O'Connor, D. V.; Philips, D. *Time-Correlated Single Photon Counting;* Academic Press: New York, 1984.

(13) Zimmermann, T.; Weigerber, P. *Proc. International Workshop on Mining Software Repositories (MSR 2004)*, 2004; p 2.

(14) Grabowski, S. J. *Annu. Rep. Prog. Chem.: Sect. C* **2006**, *102*, 131.

Acknowledgment. C.P.R. acknowledges the financial support by DST, CSIR, and BRNS-DAE. We thank Dr. Haridas Pal, Radiation & Photochemistry Division, BARC, for allowing us to use the time-resolved fluorescence instrument. We thank Dr. M. Vairamani, IICT, Hyderabad, for making the mass spectrometer available for this work. We thank both the referees for their valuable suggestions.

Supporting Information Available: The fluorescence data (S1−S3), absorption data (S4−S6), ESI/MS data (S7), and computational data (S8−S10). This material is available free of charge via the Internet at http://pubs.acs.org.

JO0700979